5. Separation of the Earth's Magnetic Field into the Drifting and the Standing Parts.

By Takesi YUKUTAKE and Hiroko TACHINAKA,

Earthquake Research Institute.

Summary

The earth's magnetic field has been separated into two types of field, the standing and the drifting fields by analysing the Gauss-Schmidt coefficients going back to the 17th century. The results show that the drifting field is mainly composed of a few low harmonics, and the standing field has a more complicated distribution.

It has been confirmed that superposition of two types of field can well approximate the distribution of the observed non-dipole fields for various epochs. Even such a large rate of increase in the intensity amounting to 50 γ/year as is observed for the Mongolian anomaly can also be accounted for by simple superposition of the two types of field. It is noteworthy that these two fields seem to have no interaction with each other, suggesting that they are of separate origin.

Introduction

The non-dipole part of the earth's magnetic field has long been believed to undergo a considerably rapid time variation, and the whole part has been treated as originating from the same source within the earth's core. However, recent investigation[1] of the non-dipole field over the past several hundred years has revealed the existence of two types of non-dipole regional anomalies, the anomalies standing at the same locality and those drifting westwards. It has been confirmed that most of the conspicuous anomalies are standing ones and that only a few exhibit drifting. Some of the standing anomalies are changing their intensity very rapidly, for example, the Mongolian anomaly has changed its intensity at a rate of 50 γ/year during the last 400 years, and the others remain constant. In the 18th century, the non-dipole field in the northern hemisphere seems to have undergone a drastic change. A strong positive anomaly in the Central Pacific almost disappeared and the Mongolian anomaly started to increase.

1) T. YUKUTAKE and H. TACHINAKA, "The Non-dipole Part of the Earth's Magnetic Field," *Bull. Earthq. Res. Inst.*, **46** (1968), 1027-1074.

We have a fairly large number of spherical harmonic analyses of the main field and its secular variation since about the 16th century.[2)3)] In this paper, by making use of these analyses, it is attempted to separate the main field into the two types of field.

2. The velocity of the drifting field

Although many of the predominant non-dipole anomalies have remained nearly at the same place during the last several hundred years, the whole distribution of the geomagnetic secular variation has been confirmed to be drifting on a global scale.[4)] The drift rate of the geomagnetic secular variation was estimated by three different methods in a previous paper.[5)] In the first place, on an assumption that the distribution of the geomagnetic secular variation rotates rigidly around the geographical axis, the mean rate was estimated to be 0.295°/year (Model A). Secondly, the scalar potentials of the geomagnetic secular variation along parallel

Table 1. Velocity models obtained from the secular variation
  A: Rigidly rotating field model
  B: Dispersive velocities for Fourier components when the potential along parallels are expanded in Fourier series
  C: Dispersive velocities for individual spherical harmonics

model A	$v_n^m = 0.295°/yr$
model B	$v_n^1 = 0.166°/yr$
	$v_n^2 = 0.339°/yr$
	$v_n^3 = 0.269°/yr$
	$v_n^4 = 0.189°/yr$
	$v_n^m = 0.3°/yr$ for $m \geqq 5$
model C	$v_1^1 = 0.297°/yr$
	$v_2^1 = 0.229°/yr$
	$v_2^2 = 0.334°/yr$
	$v_3^1 = -0.109°/yr$
	$v_3^2 = 0.733°/yr$
	$v_3^3 = 0.267°/yr$
	$v_n^m = 0.3°/yr$ for $n \geqq 4$

  2) T. Yukutake and H. Tachinaka, *loc. cit.*, 1).
  3) T. Yukutake and H. Tachinaka, "The Westward Drift of the Geomagnetic Secular Variation," *Bull. Earthq. Res. Inst.*, **46** (1968), 1075-1102.
  4) T. Yukutake and H. Tachinaka, *loc. cit.*, 3)
  5) T. Yukutake, "The Drift Velocity of the Geomagnetic Secular Variation," *J. Geomag. Geoelect.*, **20** (1968), 403-414.

circles were expanded in Fourier series and the drift rates of the individual harmonic components were examined. The mean rates over the various parallel circles were calculated for each harmonic number m (Model B). The results are reproduced in Table 1. Thirdly time variation in the longitudes of phase angles of individual spherical harmonic components was investigated (Model C). The drift velocity for each constituent is also shown in Table 1. We shall call these three different sets of velocities velocity model A, B and C respectively.

Since the geomagnetic secular variation likely gives a better approximation for the velocity of the drifting field than the main field does, one of the above three models was adopted to separate the field into two types.

3. Separation of the field into the standing and the drifting parts.

Let us assume that the magnetic potential V is composed of the standing part F_n^m and the drifting one K_n^m as follows,

$$
\left.
\begin{aligned}
V &= a \sum_n \sum_m V_n^m P_n^m (\cos \theta), \\
V_n^m &= F_n^m \cos (m\lambda + \varphi_n^m) + K_n^m \cos m\{\lambda + v_n^m (t - \tau_n^m)\}, \\
&= \{F_n^m \cos \varphi_n^m + K_n^m \cos m v_n^m (t - \tau_n^m)\} \cos m\lambda \\
&\quad - \{F_n^m \sin \varphi_n^m + K_n^m \sin m v_n^m (t - \tau_n^m)\} \sin m\lambda,
\end{aligned}
\right\} \tag{1}
$$

where $P_n^m (\cos \theta)$ is a Schmidt's half-normalized spherical function and a is the mean radius of the earth. θ and λ denote the colatitude and the east longitude respectively. F_n^m and φ_n^m are the amplitude and the phase angle of the standing component, and K_n^m, τ_n^m represent the amplitude of the drifting component and its phase measured in the unit of time. v_n^m is the drift velocity measured in 0.01°/year and t is time with the origin at 1800 A.D. defined by

$$
t = (T - 1800)/100
$$

where T is the epoch in the year A.D.

The magnetic potential is, on the other hand, customarily expressed by the Gauss-Schmidt coefficients as follows,

$$
V_n^m = g_n^m (t) \cos m\lambda + h_n^m (t) \sin m\lambda.
$$

Therefore, we have

T. Yukutake and H. Tachinaka

$$g_n^m(t) = F_n^m \cos \varphi_n^m + K_n^m \cos m v_n^m(t - \tau_n^m),$$
$$-h_n^m(t) = F_n^m \sin \varphi_n^m + K_n^m \sin m v_n^m(t - \tau_n^m). \qquad \left. \right\} \qquad (2)$$

If we select a velocity model from Table 1 for v_n^m and substitute it into equation (2), the unknown variables are F_n^m, φ_n^m, K_n^m and τ_n^m. Let us define a function ψ as follows,

$$\psi = \sum_t \{\varepsilon(t)\}^2,$$
$$\{\varepsilon(t)\}^2 = \{F_n^m \cos \varphi_n^m + K_n^m \cos m v_n^m(t - \tau_n^m) - g_n^m(t)\}^2 \qquad \left. \right\} \qquad (3)$$
$$+ \{F_n^m \sin \varphi_n^m + K_n^m \sin m v_n^m(t - \tau_n^m) + h_n^m(t)\}^2,$$

Table 2. The standing and the drifting parts of the earth's magnetic
field determined for 11 sets of data
F_n^m; amplitude of the standing component
φ_n^m; phase angle of the standing component
K_n^m; amplitude of the drifting component
τ_n^m; phase of the drifting component measured in time unit

n	m	F_n^m	φ_n^m	K_n^m	τ_n^m
1	1	3503r	$-78.4°$	3896r	9.70
2	1	1571	112.9	3570	1.31
2	2	399	139.8	1879	1.68
3	1	1667	-124.7	1907	-5.47
3	2	1076	-7.9	225	1.14
3	3	342	-39.8	540	1.36
4	1	920	25.9	556	7.26
4	2	638	34.1	121	2.42
4	3	231	118.4	252	-1.33
4	4	224	68.4	161	1.71
5	1	479	27.9	179	8.73
5	2	291	-4.0	54	-1.69
5	3	54	167.0	63	0.71
5	4	113	127.3	35	-0.65
5	5	101	-60.1	81	0.64
6	1	58	45.8	48	4.83
6	2	49	-148.5	67	2.22
6	3	154	172.1	45	-1.09
6	4	20	170.9	5	0.24
6	5	104	-95.3	55	1.03
6	6	40	-176.8	34	0.57

where the summation is taken over the data of different epochs.   Regarding $F_n^m \cos \varphi_n^m$, $F_n^m \sin \varphi_n^m$, $K_n^m \cos m v_n^m \tau_n^m$ and $K_n^m \sin m v_n^m \tau_n^m$ as independent variables, we determine them first so as to minimize the function ϕ for the Gauss-Schmidt coefficients of different epochs.   Then we can calculate F_n^m, φ_n^m, K_n^m and τ_n^m.

The results thus obtained for the velocity model B are shown in Table 2.   Eleven sets of the Gauss-Schmidt coefficients were employed for the calculation from the analyses by Fritsche (1600, 1650, 1700 and 1780), Adams (1845), Schmidt (1885), Dyson-Furner (1922), Vestine et al. (1945), Finch-Leaton (1955), Cain et al. (1960) and Leaton et al. (1965). It is noteworthy that, as far as the harmonic terms up to $n=m=3$, drifting terms (K_n^m) dominate over standing terms (F_n^m) except for $n=3$, $m=2$.   For $n=2$, $m=2$, the drifting term is several times larger than the standing one.   Even though the number of data set is increased, the figures listed in Table 2 are nearly the same.   Table 3 indicates the results when the analyses by Erman-Petersen for 1829, Gauss for 1835, Fritsche for 1842, Adams for 1880, Neumayer-Petersen for 1885, Fritsche for 1885, Fanselau-Kautzleben for 1945, Hendrics-Cain for 1960, and Cain et al. for 1965 were newly added to the previous set of data.

From the results, the standing parts of the non-dipole field were synthesized for the three components, as are shown in Figs. 1 (a) to (c), where the velocity model B is adopted for the 11 sets of data.   With

Table 3. The standing and the drifting parts of the earth's magnetic
    field determined for 20 sets of data
    F_n^m;   amplitude of the standing component
    φ_n^m;   phase angle of the standing component
    K_n^m;   amplitude of the drifting component
    τ_n^m;   phase of the drifting component measured in time unit

n	m	F_n^m	φ_n^m	K_n^m	τ_n^m
1	1	3548γ	$-83.3°$	3677γ	9.51
2	1	1610	116.5	3685	1.36
2	2	313	138.9	1830	1.70
3	1	1679	-124.4	1930	-5.41
3	2	1142	-8.3	210	0.94
3	3	276	-45.4	595	1.43
4	1	950	23.8	534	7.50
4	2	623	34.0	120	2.43
4	3	209	132.1	200	-1.28
4	4	254	74.2	176	1.81

respect to the zonal terms, it is impossible to discriminate the drifting field from the standing one. Therefore all the zonal terms are included in the standing field, though such a treatment would not be admitted when the physical source of each type of field is discussed. When the distribution of the vertical component, for example, is compared with that of the non-dipole field in Fig. 10 (a), it may be noticed that the main features of the standing anomalies are very similar to those of the non-dipole field itself. This is probably due to the fact that the most predominating anomalies such as the Mongolian and the North American anomalies are the standing ones. Figs. 2 (a) to (f) show the drifting parts of the non-dipole vertical component for various epochs from 1500 to 2000 A. D. at an interval of a hundred years. Since the dispersive velocity of model B has been adopted, the non-dipole anomalies change their distribution gradually with time. As may be expected from the preponderance of the lower harmonics in Tables 2 and 3, the distributions of the drifting fields are much simpler than the standing field, composed of several large foci. In Figs. 3 (a) and (b), the drifting parts of the non-dipole north and east components are shown only for 1900 A.D.
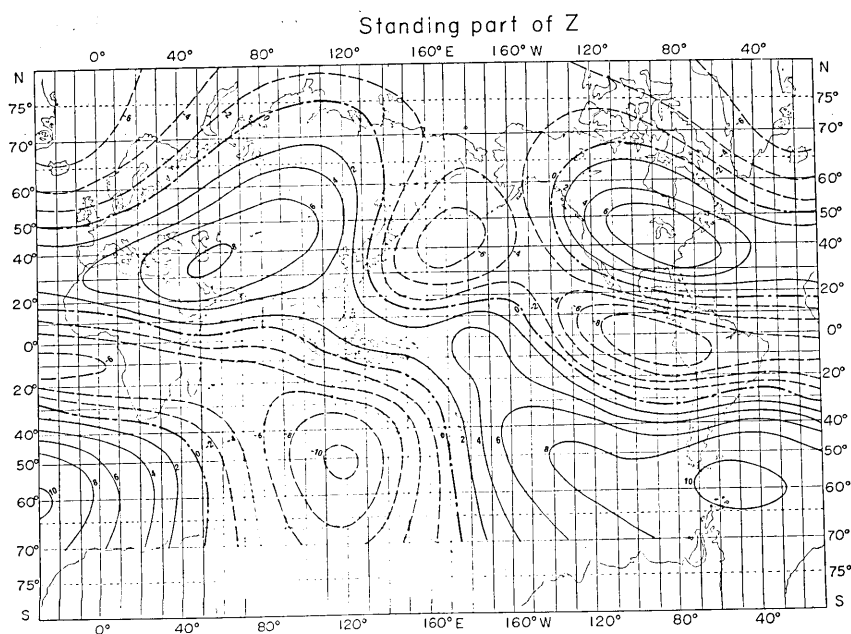
Standing part of Z

Fig. 1-(a) Standing part of the non-dipole vertical component calculated for the velocity model B, contour interval 2000 γ.
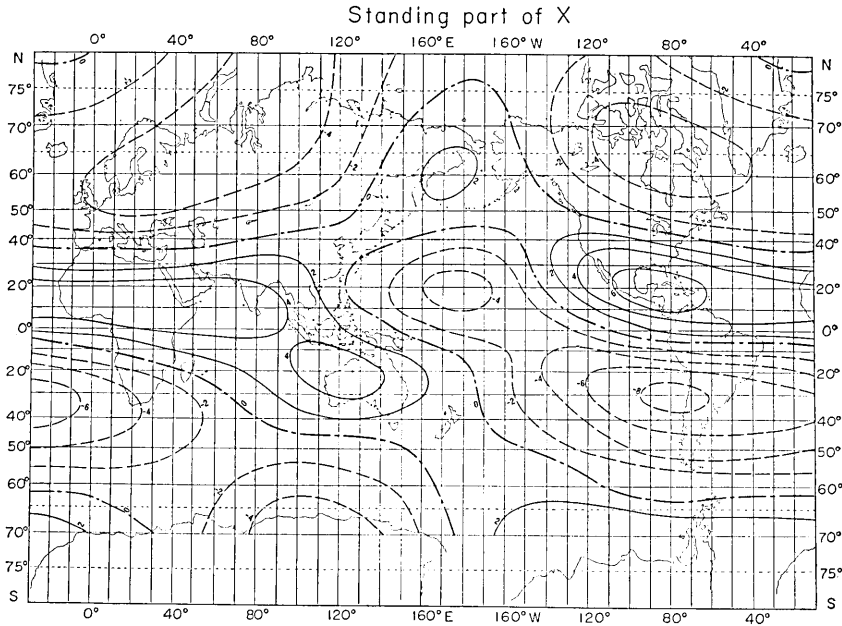
Standing part of X

Fig. 1-(b) Standing part of the non-dipole north component calculated for the velocity model B, contour interval 2000 γ.
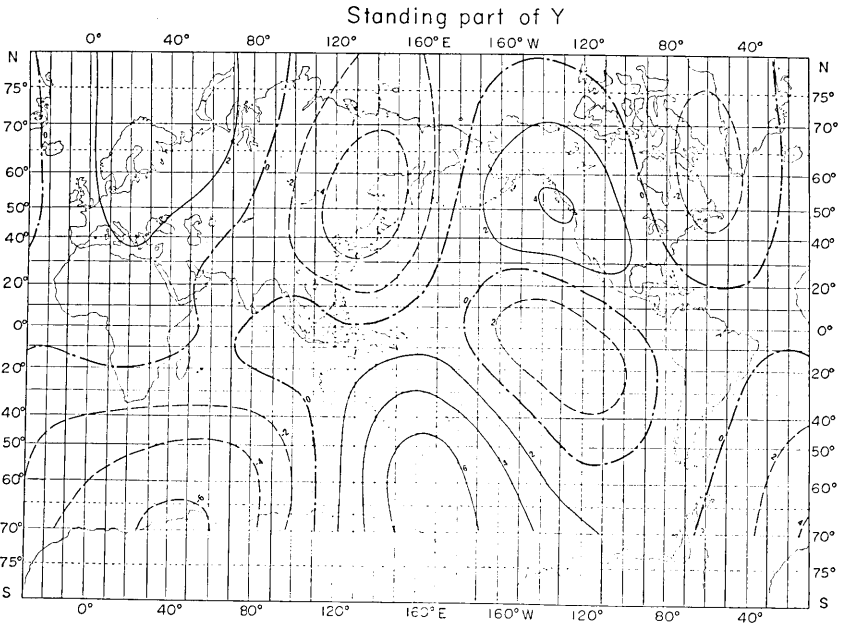
Standing part of Y

Fig. 1-(c) Standing part of the non-dipole east component calculated for the velocity model B, contour interval 2000 γ.
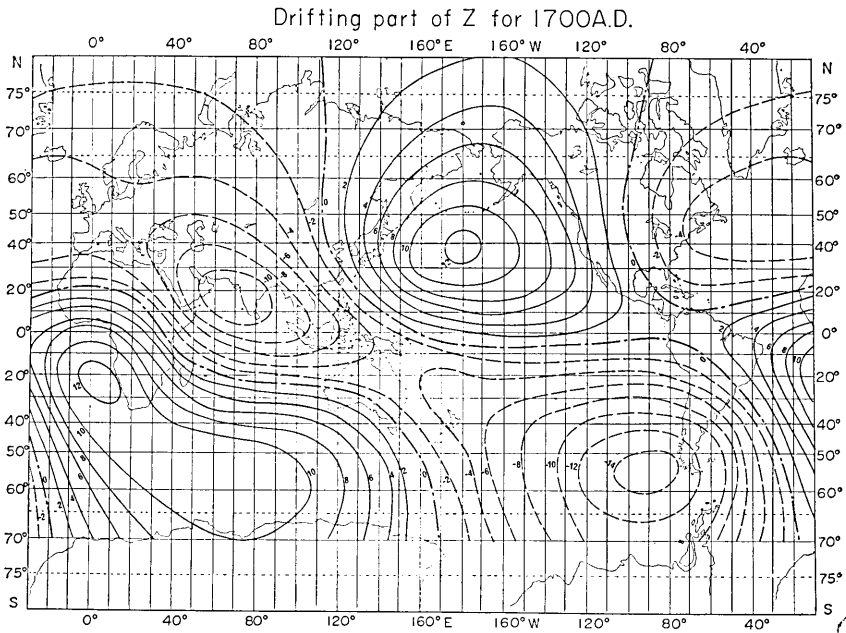
Drifting part of Z for 1500A.D.

Fig. 2-(a) Drifting part of the non-dipole vertical component for 1500 A. D., based on the velocity model B, contour interval 2000 γ.
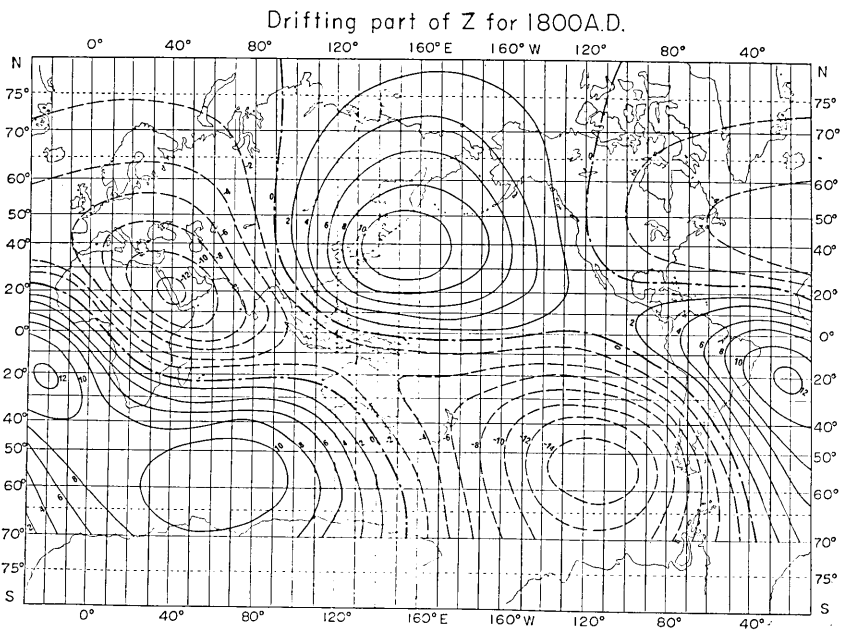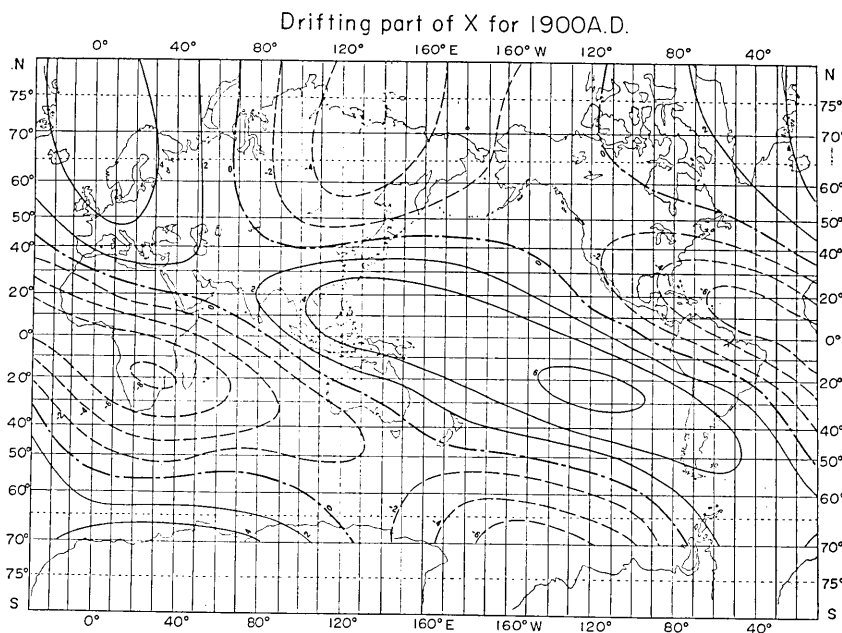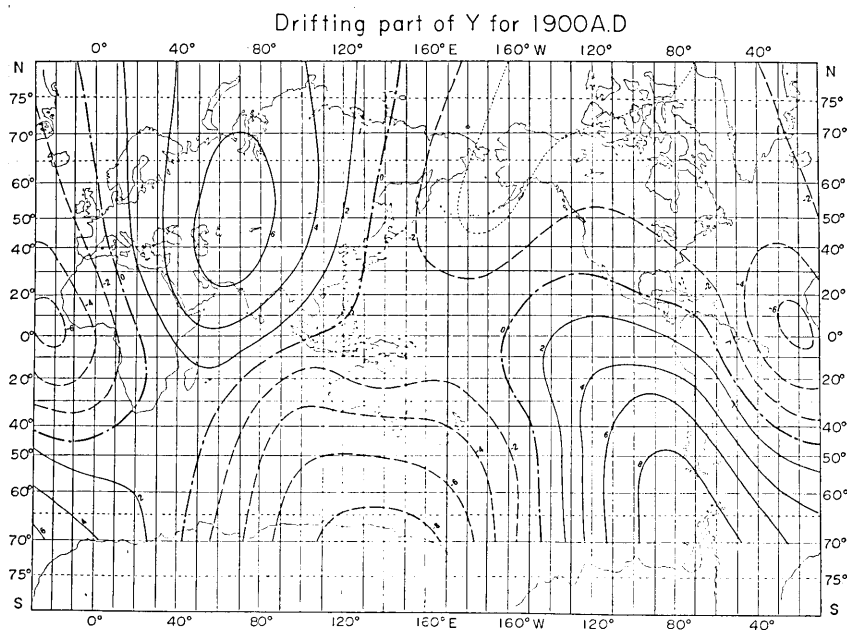
Drifting part of Z for 1600A.D.

Fig. 2-(b) Drifting part of the non-dipole vertical component for 1600 A. D., based on the velocity model B, contour interval 2000 γ.

Drifting part of Z for 1700A.D.

Fig. 2-(c)   Drifting part of the non-dipole vertical component for 1700 A. D., based on the velocity model B, contour interval 2000 γ.

Drifting part of Z for 1800A.D.

Fig. 2-(d)   Drifting part of the non-dipole vertical component for 1800 A. D., based on the velocity model B, contour interval 2000 γ.

Drifting part of Z for 1900 A.D.

Fig. 2-(e) Drifting part of the non-dipole vertical component for 1900 A. D., based on the velocity model B, contour interval 2000 γ.

Drifting part of Z for 2000 A.D

Fig. 2-(f) Drifting part of the non-dipole vertical component for 2000 A. D., based on the velocity model B, contour interval 2000 γ.

Drifting part of X for 1900A.D.

Fig. 3-(a) Drifting part of the non-dipole north component for 1900 A. D. based on the velocity model B, contour interval 2000 γ.

Drifting part of Y for 1900A.D

Fig. 3-(b) Drifting part of the non-dipole east component for 1900 A. D., based on the velocity model B, contour interval 2000 γ.
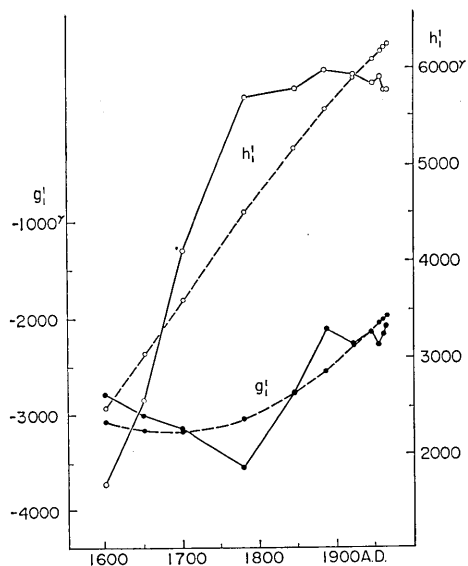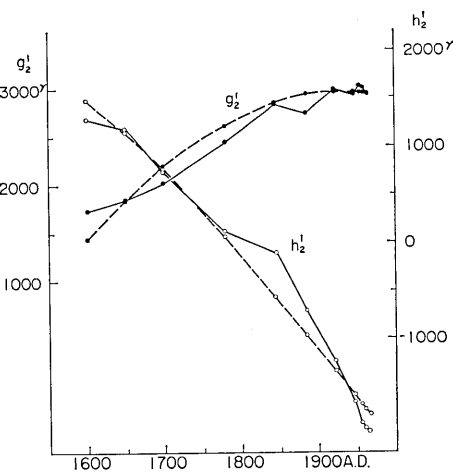
Fig. 4 (a)

Fig. 4 (b)
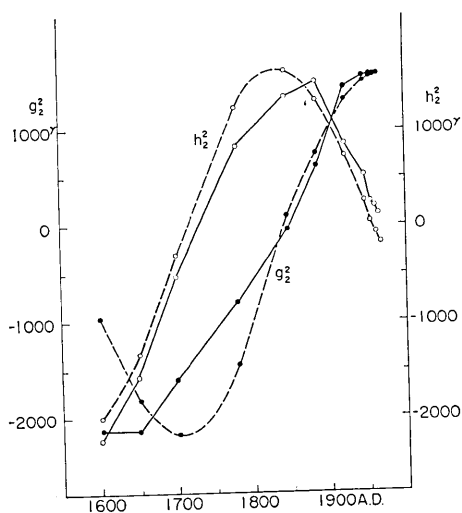
Fig. 4 (c)
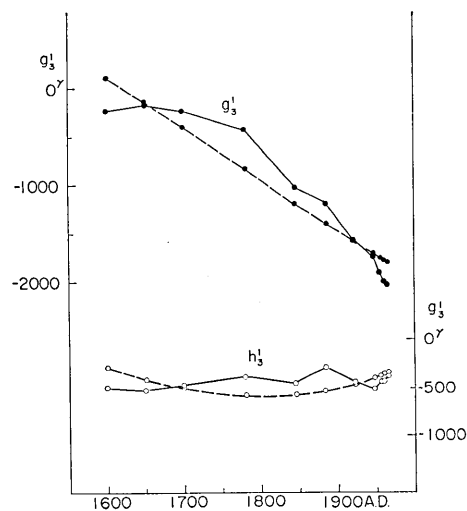
Fig. 4 (d)

Fig. 4 (a~p) Comparison of the Gauss-Schmidt coefficients between the observed and the computed. Solid circles represent g_n^m and open circles h_n^m. Observed coefficients are connected by solid lines, while the computed are by broken lines.
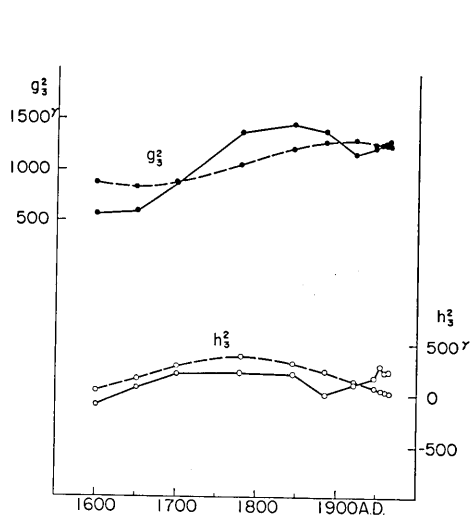
Fig. 4 (e)
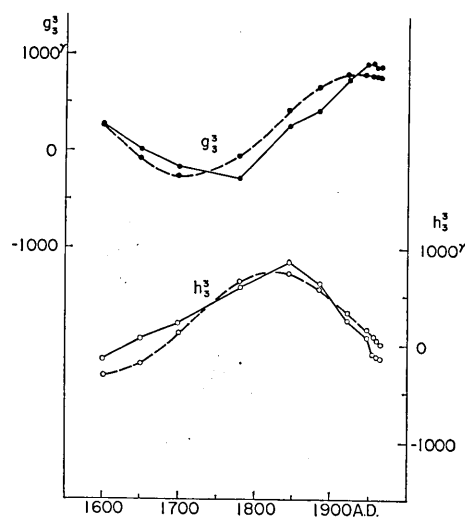
Fig. 4 (f)
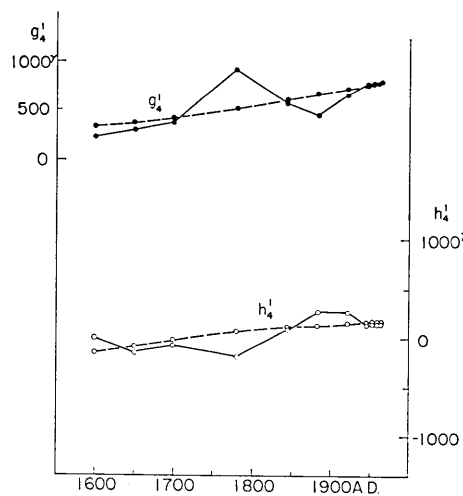
Fig. 4 (g)
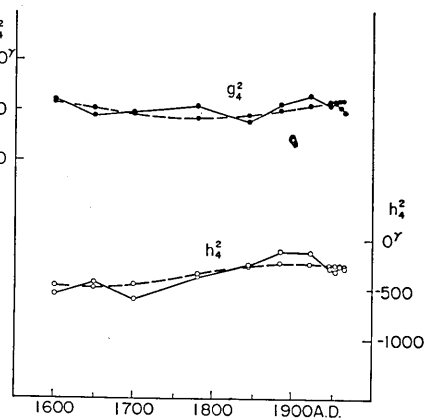
Fig. 4 (h)

4. Approximation of the field by the drifting and the standing component

Since the standing and the drifting components F_n^m, φ_n^m, K_n^m and τ_n^m have been obtained, g_n^m and h_n^m at various epochs can be calculated from equation (2). Figs. 4 (a) to (p) show the time variations of the coefficient g_n^m and h_n^m thus calculated by broken lines in comparison with those
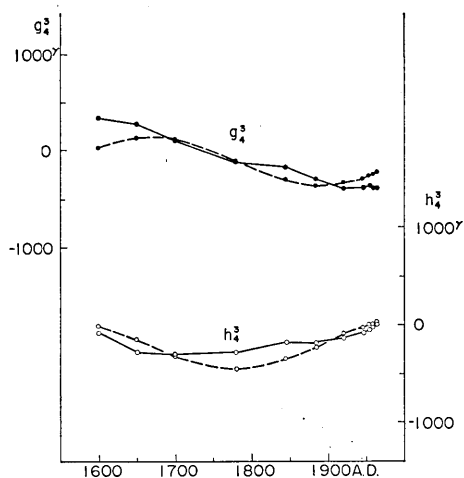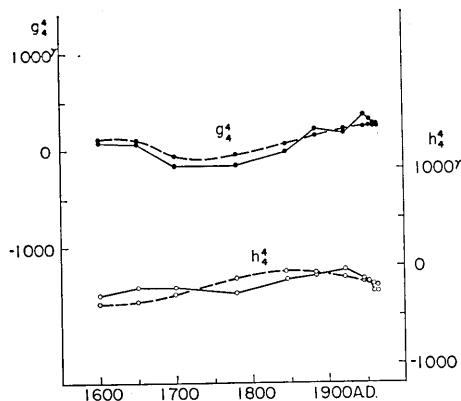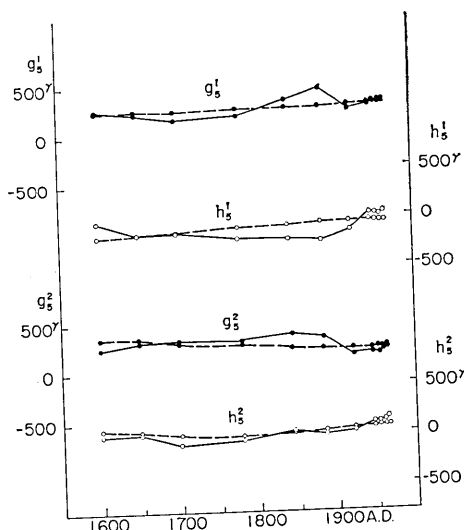
Fig. 4 (i)
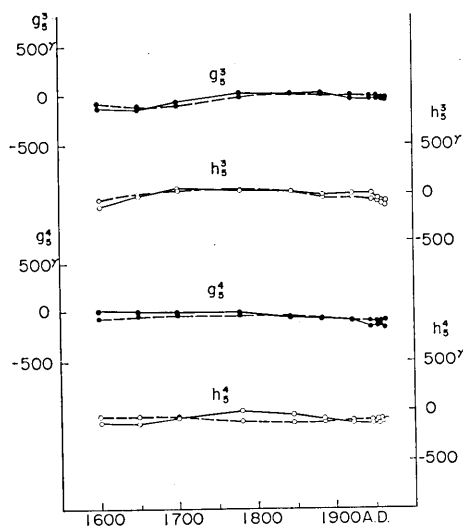

Fig. 4 (j)

Fig. 4 (k)

Fig. 4 (l)

observed connected by solid lines. The observed coefficients up to $n=3$, $m=3$ exhibit considerable variations since 1600 A.D., while those for $n=4$ have changed very moderately and the coefficients higher than $n=4$, $m=4$ have been almost constant during the period. The approximation is rather poor for h_1^1, but for other terms the agreement between the observed and the calculated is fairly good.

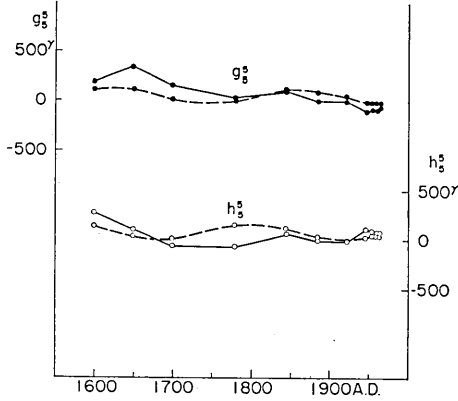Let δg_n^m, δh_n^m be differences of respective coefficients between the
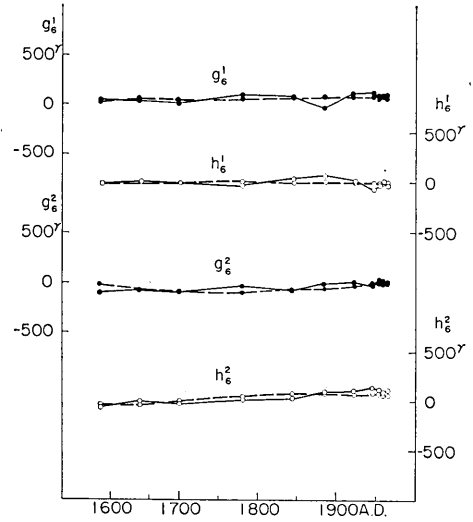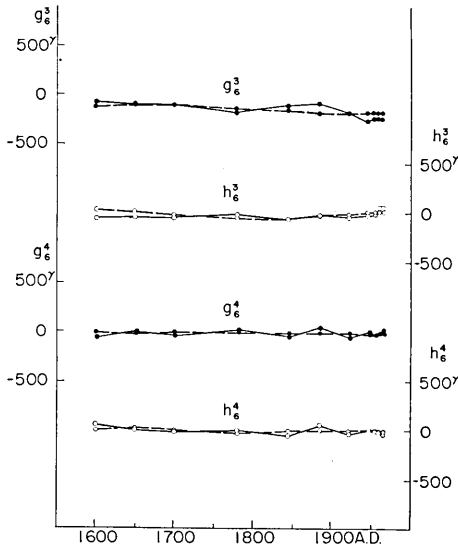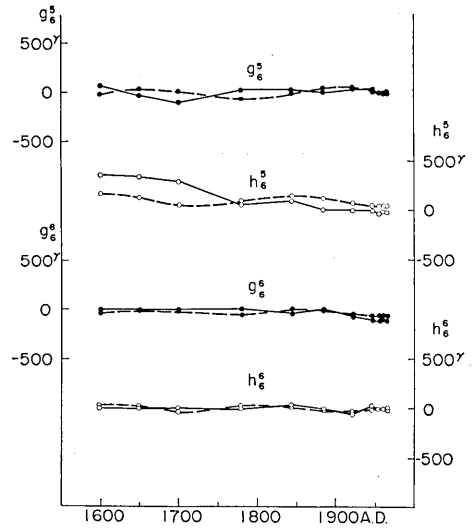
Fig. 4 (m)

Fig. 4 (n)

Fig. 4 (o)

Fig. 4 (p)

observed and the computed, and we calculate root-mean-square values of the differences. In the first place the root-mean-square difference for each harmonic component are calculated by taking the average over the period from 1600 to 1965. Let us define the root-mean-square differences of the magnetic potential $\langle \Delta V^2 \rangle_t$, those of the vertical force $\langle \Delta Z^2 \rangle_t$ and

a kind of the total force $\langle \Delta F^2 \rangle_t$ by the following equations,

$$
\begin{aligned}
\langle \Delta V^2 \rangle_t &= \left[\frac{1}{N_t} \sum_t \{ (\delta g_n^m)^2 + (\delta h_n^m)^2 \} \right]^{1/2} , \\
\langle \Delta Z^2 \rangle_t &= \left[\frac{1}{N_t} \sum_t \frac{(n+1)^2}{2n+1} \{ (\delta g_n^m)^2 + (\delta h_n^m)^2 \} \right]^{1/2} , \\
\langle \Delta F^2 \rangle_t = \langle \Delta X^2 + \Delta Y^2 + \Delta Z^2 \rangle_t &= \left[\frac{1}{N_t} \sum_t (n+1) \{ (\delta g_n^m)^2 + (\delta h_n^m)^2 \} \right]^{1/2} ,
\end{aligned}
\tag{4}
$$

where summation is made for the data of different epochs and N_t is the number of data for different epochs. The root-mean-square values of the above three quantities were computed for the 11 epoch data which had been already used for the separation of the drifting field from the standing one. In Table 4 only $\langle \Delta Z^2 \rangle_t$ is shown for the three velocity models. The approximation of the field is the worst for the term $n=1$, $m=1$ and the term $n=2$, $m=2$ is the next for the three velocity models.

In the second place, specifying an epoch, root-mean-square differences for respective epochs were calculated by summing up the square differences all over the harmonics. For the vertical component, for example, we calculated $\langle \Delta Z^2 \rangle_{n,m}$ defined by,

$$
\langle \Delta Z^2 \rangle_{n,m} = \left[\frac{1}{N} \sum_n \sum_m \frac{(n+1)^2}{2n+1} \{ (\delta g_n^m)^2 + (\delta h_n^m)^2 \} \right]^{1/2} ,
\tag{5}
$$

where N is the total number of the spherical harmonic terms. Similarly $\langle \Delta V^2 \rangle_{n,m}$ and $\langle \Delta F^2 \rangle_{n,m}$ were computed for the 11 different epochs. Table 5 shows the results of $\langle \Delta Z^2 \rangle_{n,m}$ for the different velocity models. The approximation is the best for 1922, the next for 1945 and the worst for 1600. No systematic time variations in the root-mean-square differences of the vertical forces are observable.

Similar examinations were repeated for the spherical harmonic coefficients of the secular variation. From equation (2), we have the following equations for the spherical harmonic coefficients of the geomagnetic secular variation.

$$
\begin{aligned}
\dot{g}_n^m(t) &= -m v_n^m K_n^m \sin m v_n^m (t - \tau_n^m), \\
\dot{h}_n^m(t) &= -m v_n^m K_n^m \cos m v_n^m (t - \tau_n^m).
\end{aligned}
\tag{6}
$$

In Figs. 5 (a) to (g), the harmonic coefficients computed from equation (6), by adopting the velocity model B for v_n^m, are compared with the observed ones. The computed values approximate the general trends of time variation in the coefficients fairly well as can be seen in the sectorial terms, $n=2$, $m=2$ and $n=3$, $m=3$. But the approximation is

Table 4. Root-mean-square differences in the vertical component averaged in time, $\langle \Delta Z^2 \rangle_t$, for the three velocity models.

n	m	Model A	Model B	Model C
1	1	687r	726r	687r
2	1	404	328	355
2	2	499	701	675
3	1	431	375	329
3	2	343	356	445
3	3	296	294	295
4	1	312	297	313
4	2	174	175	174
4	3	330	277	340
4	4	246	191	250
5	1	221	216	221
5	2	160	161	160
5	3	91	90	92
5	4	118	126	116
5	5	257	251	251
6	1	97	98	97
6	2	89	100	90
6	3	138	131	139
6	4	87	88	87
6	5	276	275	275
6	6	83	83	83
Mean		298	308	317

Table 5. Root-mean-square differences in the vertical component averaged for all the harmonic terms $\langle \Delta Z^2 \rangle_{n,m}$, indicating time variation in the root-mean-square differences.

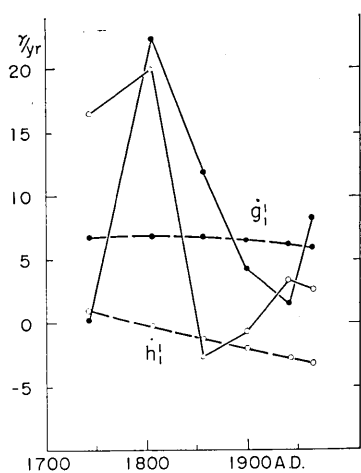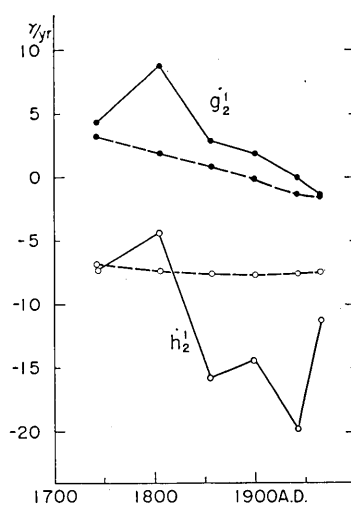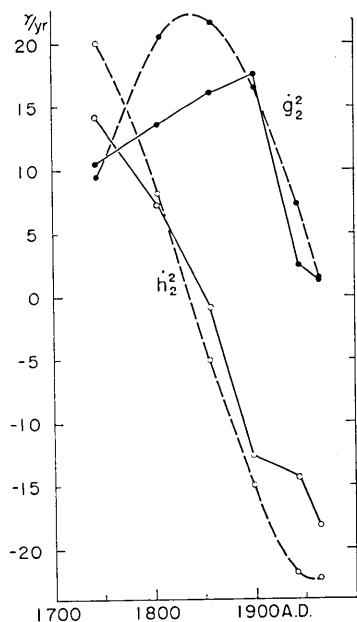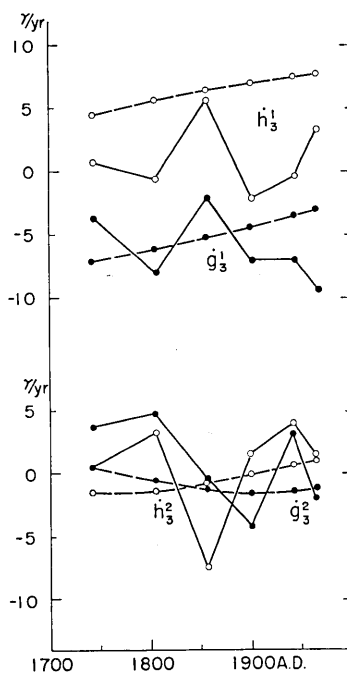| Epoch	Model A	Model B	Model C
1600	454r	502r	530r
1650	277	275	304
1700	300	285	318
1780	473	514	469
1845	273	294	292
1885	328	308	316
1922	141	140	144
1945	173	178	180
1955	209	197	196
1960	223	221	214
1965	231	233	228
Mean	298	308	312

Fig. 5 (a)

Fig. 5 (b)

Fig. 5 (c)

Fig. 5 (d)

Fig. 5 (a~g) Comparison of the spherical harmonic coefficients of the geomagnetic
secular variation. Solid circles represent $\dot{g}_n^m$ and open ones $\dot{h}_n^m$. Observed coefficients are
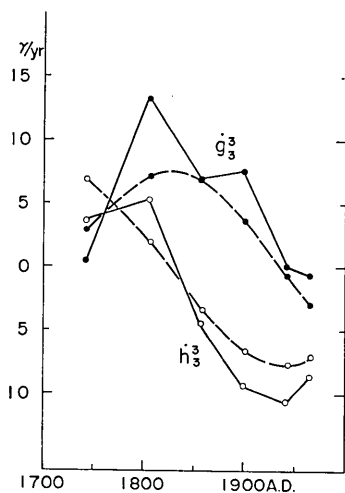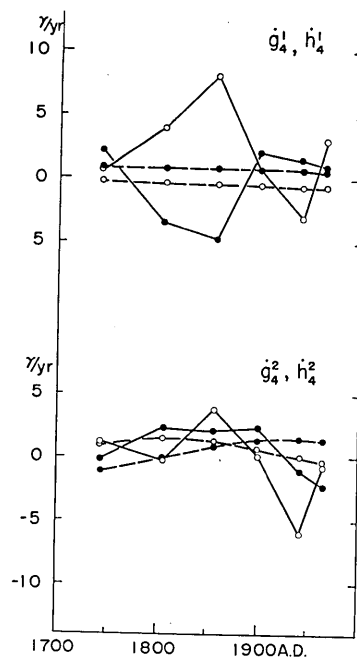connected by solid lines, and the computed by broken lines.
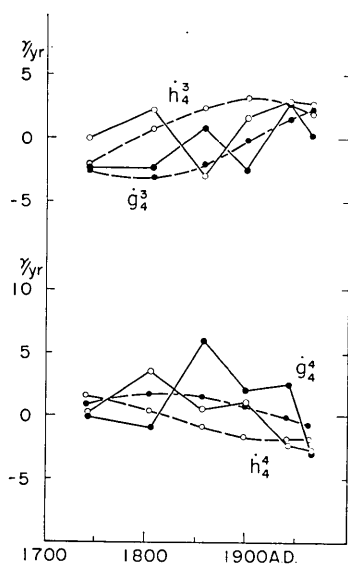
Fig. 5 (e)

Fig. 5. (f)

Fig. 5 (g)

definitely worse than in the case of the main field.

The root-mean-square differences of the vertical component for respective harmonic constituents were computed for the secular variation as are listed in Table 6. For the velocity model A, the fitness is the worst for $n=3$, $m=1$ and the next for $n=1$, $m=1$. For model B, it is the worst for $n=1$, $m=1$ and the next for $n=3$, $m=1$ and for model C the worst fit is seen for $n=1$, $m=1$ and the next is for $n=3$, $m=2$. It should be noted that, excepting the terms $n=3$, $m=1$ and $n=4$, $m=3$, model A (a rigid rotation model) shows the best fit among the three velocity models as in the case of the

approximation of the main field. This seems to suggest that such a distribution of the secular variation as may be expressed by the spherical harmonic term $n=3$, $m=1$ drifts with a different rate from the rest of the field whose motion can well be approximated by a rigid rotation.

Table 6. Root-mean-square differences of the secular variation in the vertical component for respective harmonic constituents, $\langle \Delta Z^2 \rangle_t$. Comparison is made for different velocity models.

n	m	Model A	Model B	Model C
1	1	13.2γ/year	15.2γ/year	13.3γ/year
2	1	7.1	10.0	7.7
2	2	7.4	8.8	8.4
3	1	31.8	11.1	6.3
3	2	7.7	7.7	9.9
3	3	5.9	6.3	6.4
4	1	8.5	8.8	8.5
4	2	5.5	5.9	5.6
4	3	5.9	5.2	6.1
4	4	4.4	5.4	4.3
Mean		12.4	8.9	8.0

Table 7. Root-mean-square differences of the secular variation in the vertical component averaged for all the harmonic terms, $\langle \Delta Z^2 \rangle_{n,m}$.

Epoch	Model A	Model B	Model C
1743	9.4γ/year	7.8γ/year	4.4γ/year
1806	14.8	12.6	10.7
1857	12.2	9.5	10.8
1900	12.0	6.8	6.1
1942.5	12.8	9.4	7.9
1965	12.7	6.0	5.9
Mean	12.4	8.9	8.0

Table 7 shows the root-mean-square differences of the secular variation in the vertical component when summation is taken all over the harmonics. The best fit is seen for 1965 and the worst for 1806 for the first two models and for the model C the best for 1743 and the worst for 1857. In this case, the velocity model A gives the worst fit for all the epochs among the three velocity models mostly caused by a poor fit to the $n=3$, $m=1$ term. In the case of the secular

variation, too, any systematic time variation cannot be recognized, suggesting that the root-mean-square differences listed probably arise from the inaccuracy of the analyses or the errors involved in the data.

The over all root-mean-square differences summed up both for all the harmonics and for the different epochs were computed by the following equations.

$$
\begin{aligned}
\langle \Delta V^2 \rangle &= \left[\frac{1}{N \cdot N_t} \sum_t \sum_n \sum_m \{ (\delta g_n^m)^2 + (\delta h_n^m)^2 \} \right]^{1/2}, \\
\langle \Delta Z^2 \rangle &= \left[\frac{1}{N \cdot N_t} \sum_t \sum_n \frac{(n+1)^2}{2n+1} \sum_m \{ (\delta g_n^m)^2 + (\delta h_n^m)^2 \} \right]^{1/2}, \\
\langle \Delta F^2 \rangle &= \left[\frac{1}{N \cdot N_t} \sum_t \sum_n (n+1) \sum_m \{ (\delta g_n^m)^2 + (\delta h_n^m)^2 \} \right]^{1/2}.
\end{aligned}
\qquad (7)
$$

The results are shown in Table 8 for the respective velocity models. It can be noted that the approximation is slightly better when model A (a rigid rotation model) is adopted than in the case when any other models are used for separation of the field. Model B gives the next fit, but the difference between the root-mean-square values obtained from model B and C is very small. Similarly the root-mean-square differences for the secular variation are listed in Table 9, indicating that model C gives the best fit for the secular change and model A the worst. From Tables 8 and 9, it is seen that model B gives equally better approximation both for the main field and the secular variation. Therefore the separated fields by model B is finally adopted in this study.

Table 8. Root-mean-square differences of the main field for the three velocity models.

	$\langle \Delta V^2 \rangle$	$\langle \Delta Z^2 \rangle$	$\langle \Delta F^2 \rangle$
Model A	212γ	298γ	387γ
B	223	308	400
C	223	312	405

Table 9. Root-mean-square difference of the secular variation for the three velocity models.

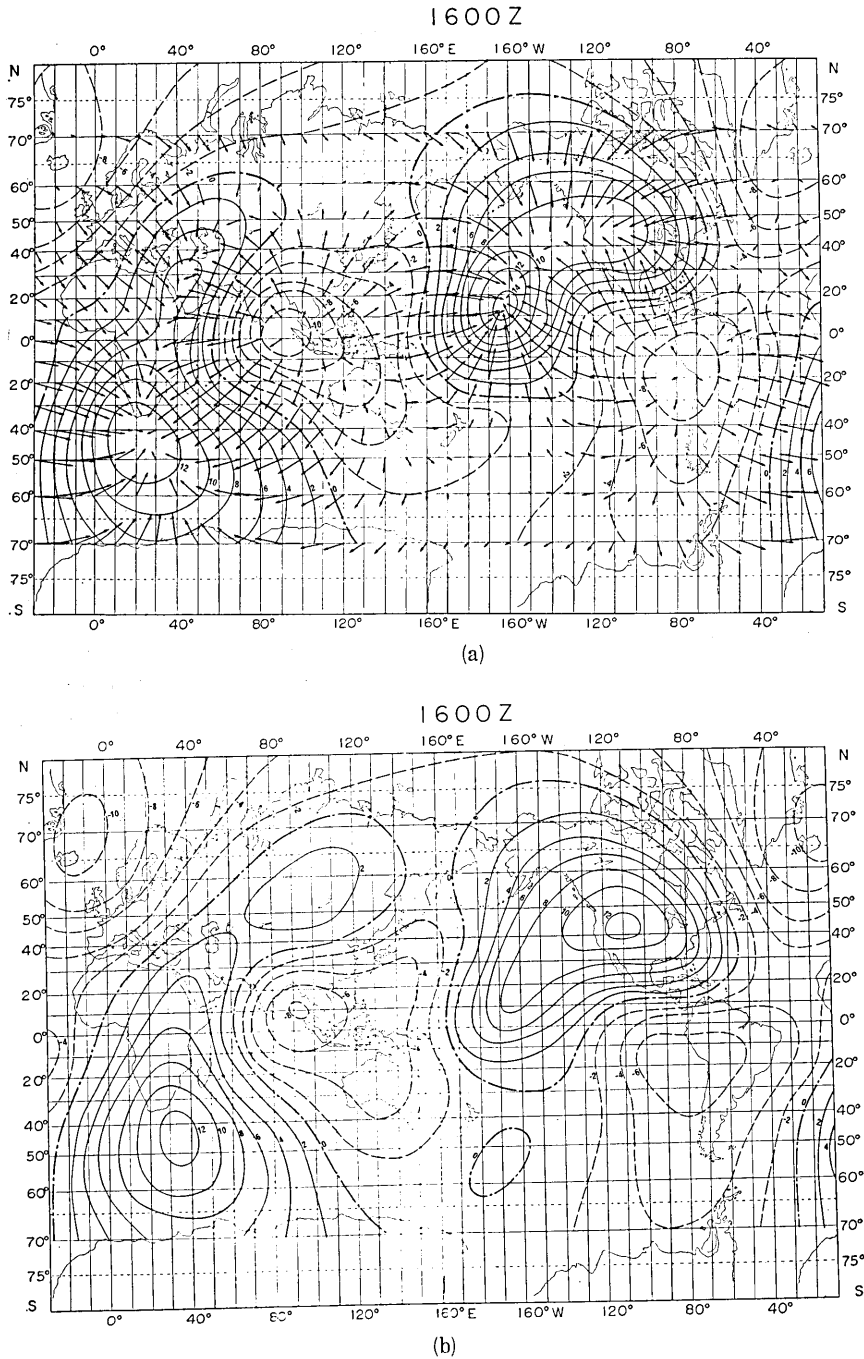|	$\langle \Delta V^2 \rangle$	$\langle \Delta Z^2 \rangle$	$\langle \Delta F^2 \rangle$
model A	8.5γ/year	12.4γ/year	16.3γ/year
B	6.6	8.9	11.6
C	5.8	8.0	10.4

1600 Z

(a)

1600 Z

(b)

Fig. 6 The non-dipole field for 1600 A. D. (vertical component) (a) the observed field.
(b) the computed field from the standing and drifting parts (for velocity mcdel B). Contour interval 2000 γ.
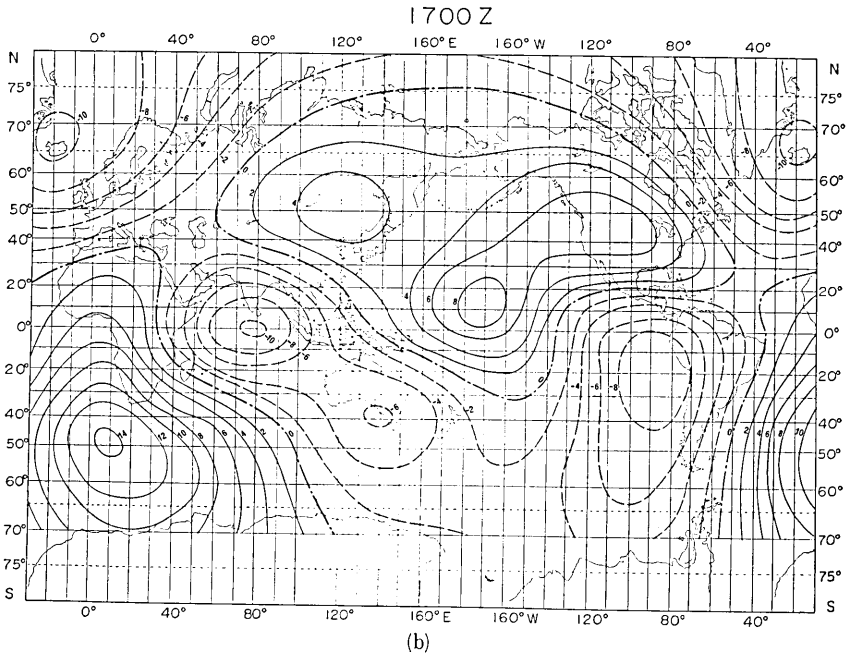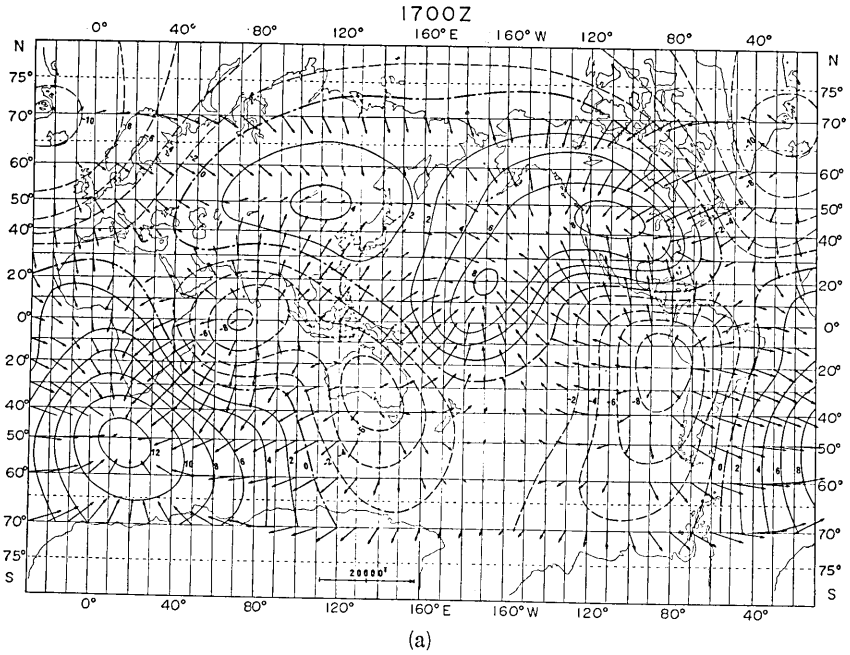
(a)

(b)

Fig. 7   The non-dipold field for 1700 A. D. (vertical component). (a) the observed field.
(b) the computed field from the standing and drifting parts (for velocity medel B).   Con-
tour interval 2000 γ.

Fig. 8 The non-dipole field for 1780 A. D. (vertical component).   (a) the observed field. (b) the computed field from the standing and drifting parts (for velocity model B). Contour interval 2000 γ.
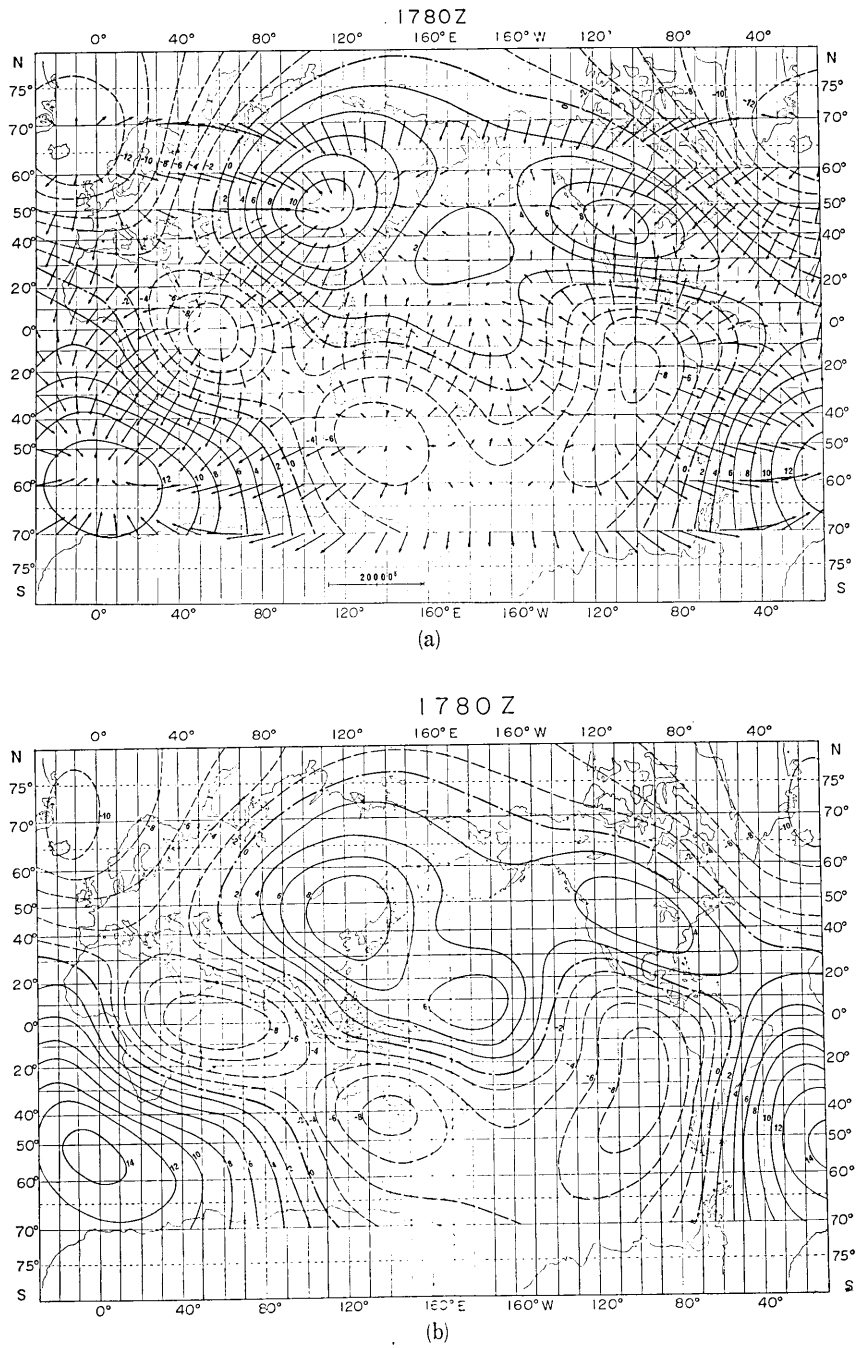
(a)

(b)

Fig. 9 The non-dipole field for 1885 A. D. (vertical component). (a) the observed field. (b) the computed field from the standing and drifting parts (for velocity model B). Contour interval 2000 γ.

Fig. 10   The non-dipole field for 1965 A. D. (vertical component).   (a) the observed field.   (b) the computed field from the standing and drifting parts (for velocity model B). Contour interval 2000 γ.
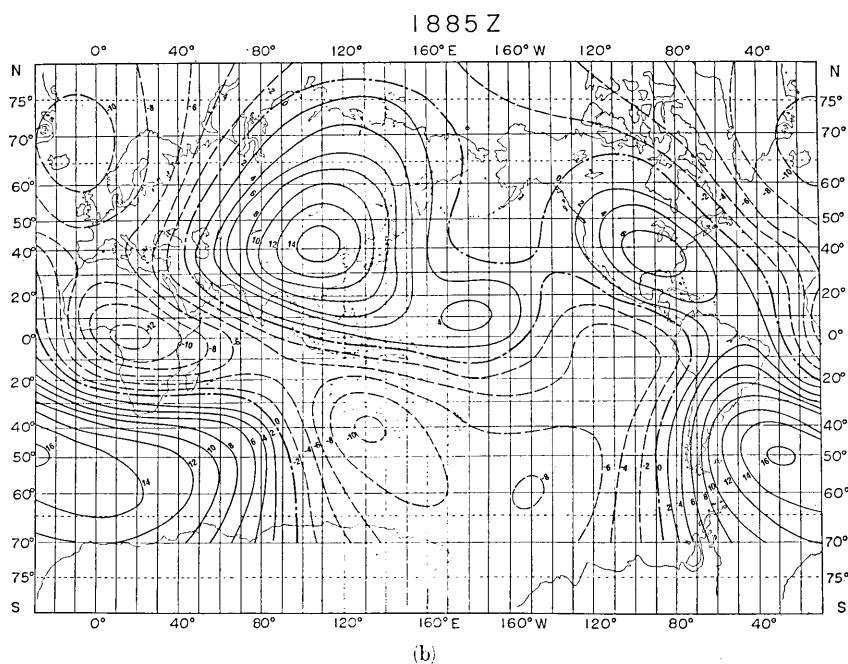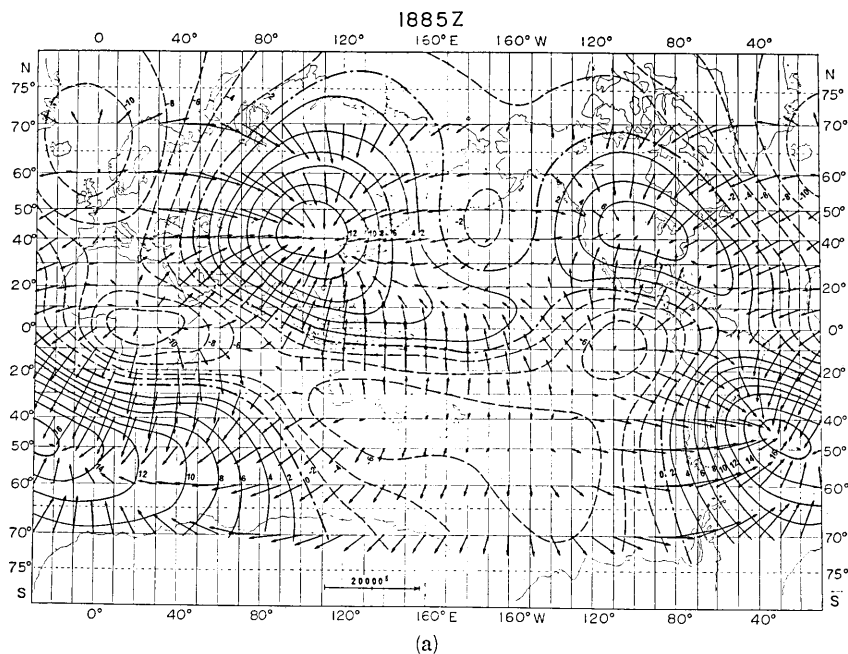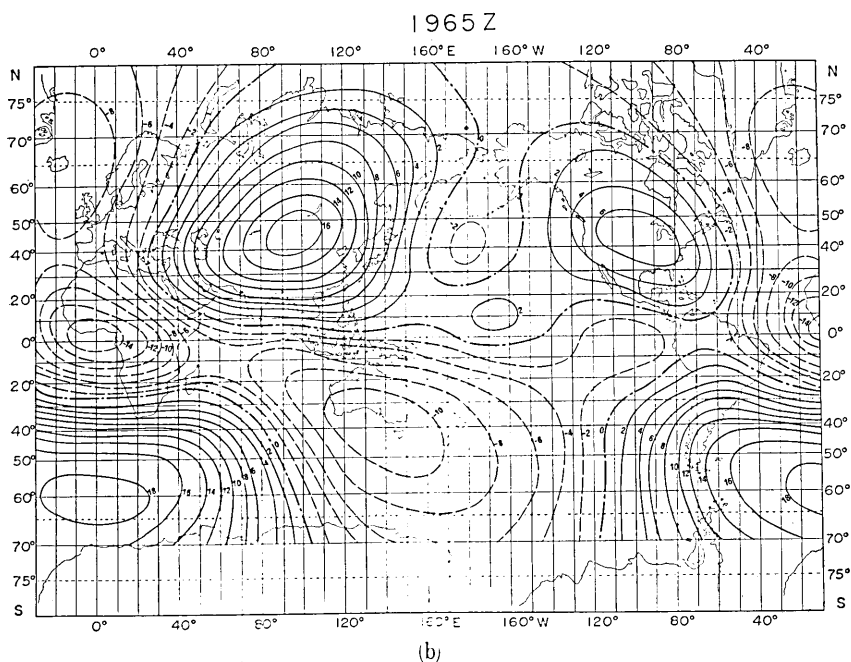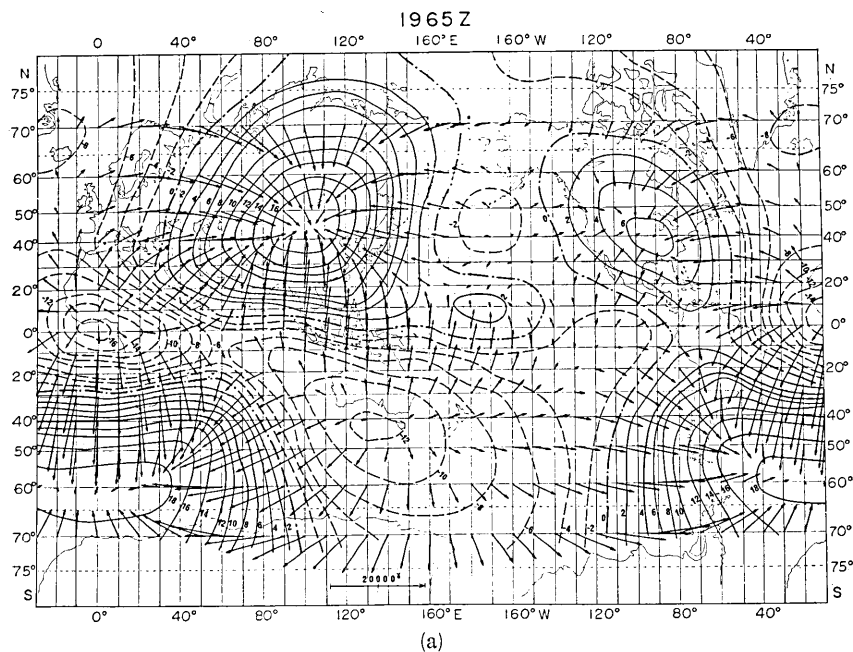
5. The non-dipole field synthesized from the drifting and the standing parts

In the previous section, we examined how closely the coefficients computed from the drifting and the standing parts can approximate the observed Gauss-Schmidt coefficients. In this section, a more direct comparison is made. The non-dipole fields are synthesized from the synthetic coefficients. As for the zonal components, we have simply employed the observed values for the respective epochs. Figs. 6 to 10 are the comparison of the non-dipole vertical fields thus synthesized with the observed for the epochs 1600, 1700, 1780, 1885 and 1965.

Fig. 11   Variation of the Mongolian positive anomaly with time. From the top to the bottom, time variation in the intensity at the center of the anomaly, variations in the longitude and the latitude of the center. Solid circles are obtained from the observed charts and open ones from the computed.
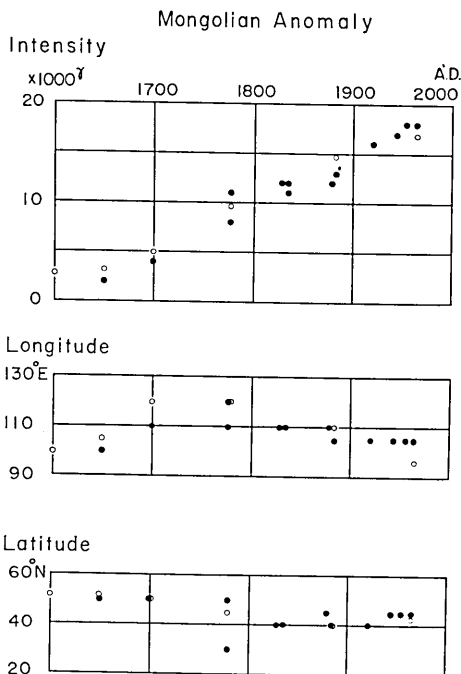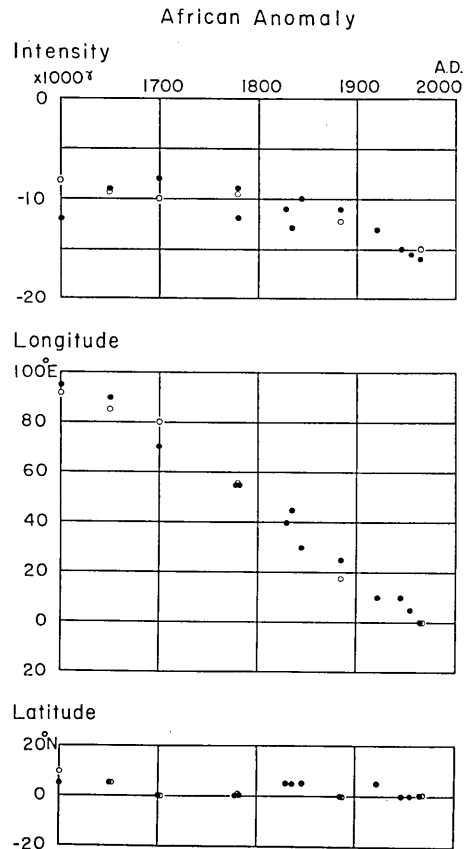
Fig. 12   Variation of the African negative anomaly with time. From the top to the bottom, time variation in the intensity at the center of the anomaly, variations in the longitude and the latitude of the center. Solid circles are obtained from the observed charts and open ones from the computed.

The individual features of the non-dipole fields are well represented in the computed charts. In the observed chart for 1965 (Fig. 10 (a)), for example, there are five large anomalies (Mongolian positive, North American positive, South Atlantic positive, African negative and Australian negative), three small ones (North Pacific negative, Central Pacific positive and Icelandic negative) and one intermediate anomaly in the Southeast Pacific. Corresponding to these, we can see in the computed chart, Fig. 10 (b), positive and negative anomalies whose locations and intensities are very similar to those in the observed chart.

Examination of Figs. 6 to 10 indicates that the synthetic charts well approximate not only the spatial distribution of the non-dipole
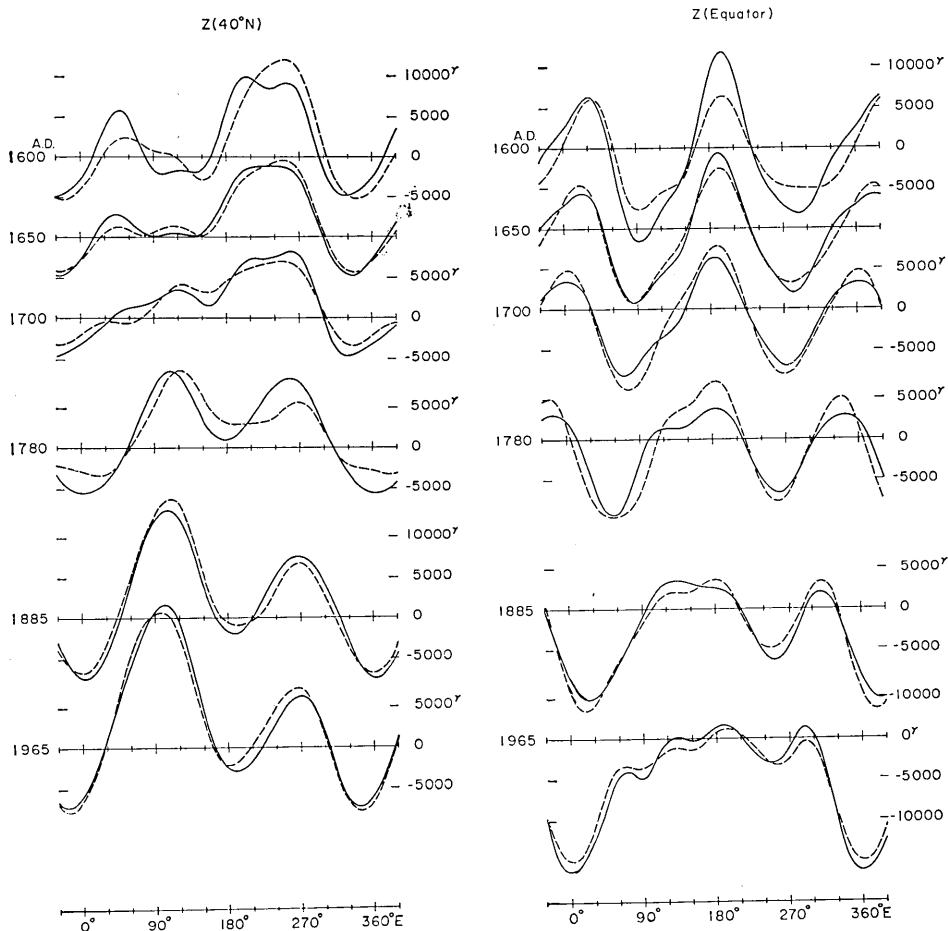
Fig. 13 (a) Profiles along 40°N circle.   Fig. 13 (b) Profiles along the equator.

Fig. 13 Non-dipole vertical fields along parallel circles for various epochs. Solid lines represent the observed magnetic profiles, while broken lines the computed from the drifting and the standing parts.

fields but also the time variations of the individual anomalies. An apparently drastic change in the distribution of the non-dipole anomalies that seems to have taken place in the 18th century can be observed in these synthesized figures. It is rather surprising to see such a rapid increase in the intensity as is observed for the Mongolian anomaly (50 γ/year) being well approximated merely by superposing a steadily drifting field on a standing field. Fig. 11 shows the variations in the intensity and the location of the center of the Mongolian anomaly. Solid circles represent the intensities and locations read from the observed charts for respective epochs, and open circles those from the computed charts. Time variation of the African negative anomaly is shown in Fig. 12. The steady westward drift with increasing absolute intensity is well approximated. In addition, about 50% increase in the absolute intensity during the period from 1600 to 1965 is also obtained from the computed charts.
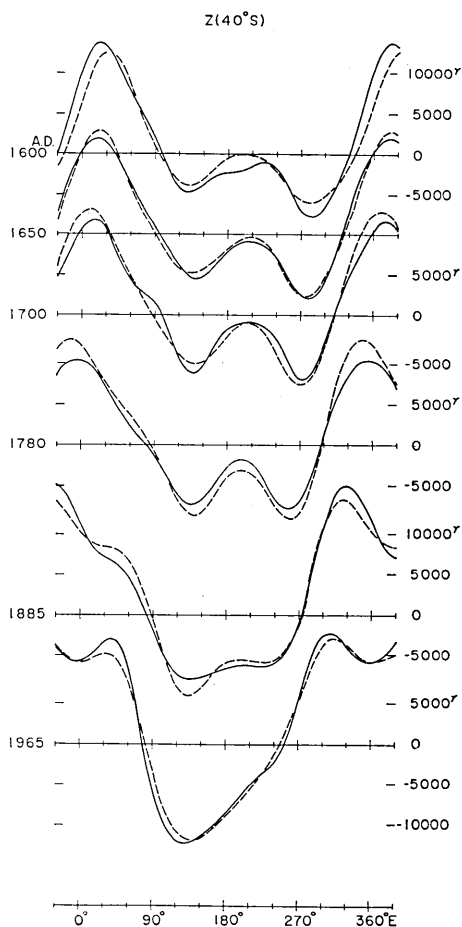
More detailed variations of the non-dipole field are observable in the profiles of the non-dipole vertical force along parallel circles for various epochs as in Figs. 13 (a) to (c) where those along the parallels 40°N, the equator and 40°S are shown. The broken lines represent the profiles synthesized from the drifting and the standing fields, while the solid lines those of the observed field. Agreements between the broken and the solid lines are generally good. For the profiles along the 40°N circle, such conspicuous features of the secular variation as disappearance of a peak that existed near 50°E in 1600 and a rapid increase of a positive peak near 100°E caused by the Mongolian anomaly are well expressed by the synthesized field. For the equator the westward drift of a steep trough produced by the African negative anomaly and disappearance of a postivie peak near

Fig. 13 (c) Profiles along 40°S circle.

200°E are well represented by broken lines.

The data treated in this analysis covers only a quarter of the whole period required for the fastest mode of the field to complete its rotation around the earth's axis. Therefore it is not very certain how far the present standing and the drifting field can approximate the observed field when they are synthesized by extrapolating beyond a 400 year period, but within the period treated here, superposition of the steady two parts can approximate the observed field fairly well.

6. Drift velocities of the spherical harmonic components for the main field

When the individual harmonic coefficients of the main field are composed of the standing and the drifting components, the drift velocities for the respective harmonic components are, as a matter of course, different from those of the drifting components. Let g_n^m, h_n^m be the spherical harmonic coefficients for the main field and $\dot{g}_n^m$, $\dot{h}_n^m$ be those for the secular variation. Then the westward drift velocity (u_n^m) for the main field is computed as follows,[6]

$$u_n^m = -\frac{1}{m} \frac{g_n^m \dot{h}_n^m - h_n^m \dot{g}_n^m}{(g_n^m)^2 + (h_n^m)^2}. \tag{8}$$

On substituting equation (2) and (6), we have

$$u_n^m = v_n^m \left[1 - \frac{F_n^{m2} + F_n^m K_n^m \cos\{mv_n^m(t-\tau_n^m) - \varphi_n^m\}}{F_n^{m2} + K_n^{m2} + 2F_n^m K_n^m \cos\{mv_n^m(t-\tau_n^m) - \varphi_n^m\}} \right]. \tag{9}$$

Accordingly as the intensity of the standing field varies, the drift velocity u_n^m changes from zero to v_n^m. It is noteworthy that u_n^m is dependent on time t, while no time variation is assumed for the drift velocity v_n^m of the drifting field.

u_n^m's were calculated for 1960 and compared with the drift velocities for 1965 obtained by substituting Leaton et al.'s analysis[7] for both the main field and the secular variation into equation (8). u_n^m's obtained on the basis of velocity model B for v_n^m are listed in Table 10, together with those calculated from Leaton et al.'s analysis.

Comparison of Table 1 with Table 10 indicates a remarkable difference between the velocity for the main field (u_n^m) and that for the drifting

---

6) T. Yukutake, "Two Methods of Estimating the Drift Rate of the Earth's Magnetic Field," J. Geomag. Geoelect., 20 (1968), 427-428.

7) B. R. Leaton, S. R. C. Malin and M. J. Evans, "An Analytical Representation of the Estimated Geomagnetic Field and Its Secular Change for the Epoch 1965.0," J. Geomag. Geoelect., 17 (1965), 187-194.

Table 10. Drift rates of individual spherical harmonic components of the main field.

u_n^m; drift rates for 1960 calculated from the present model of drifting and standing field.

$u_n'^m$; drift rates obtained from Leaton et al.'s analyses both for the main field and the secular variation for 1965.

n	m	u_n^m	$u_n'^m$
1	1	0.09°/year	0.08°/year
2	1	0.16	0.16
2	2	0.40	0.33
3	1	0.11	0.14
3	2	0.05	−0.04
3	3	0.17	0.18
4	1	0.01	−0.19
4	2	0.01	0.09
4	3	0.16	0.13
4	4	0.07	0.16

Westward velocity is taken positive.

field (v_n^m). The drift velocity of the total equatorial dipole field becomes very slow (0.09°/year), while the drift rate for $n=m=1$ of the drifting field is 0.17°/year. Agreements between the drift rates computed from the present model and those obtained from Leaton et al.'s analysis seems sufficiently good when it is remembered that the present model is concerned with a considerably long period variation over several hundred years, whereas Leaton et al.'s analysis is rather based on instantaneous data that may be affected by relatively short period variations. Therefore little significance may be attached to the discrepancies for such higher terms as $n=4$. For $n=3$, $m=2$, the westward velocity is obtained from the present calculation, whereas Leaton et al.'s analysis gives eastward drift. However, both of the absolute values are so small that it is not certain whether or not there is any significance in the opposite sign of drift velocities.

7. Concluding remarks

Employing the results of the spherical harmonic analyses conducted for the past 400 years, the earth's magnetic field has been separated into two parts, the standing field and the drifting one. For simplicity, the amplitude of each harmonic term of these two types of field has been assumed to be constant. But it has been revealed that simple

superposition of these time invariant fields can well account for the
main features of the secular variations of the non-dipole field, including
such a remarkable change in the intensity of the Mongolian anomaly.
Examination of the root-mean-square differences between the observed
and the calculated field in Tables 5 and 7 does not give any significant
time variations, only indicating that these differences are likely to be
caused by inaccuracy of data and analyses. These suggest that the two
types of field obtained in this paper have long been stable and steady.

It should be noted that the earth's dipole component has reduced
its intensity about 7%, amounting to 2000γ, during the past century
and that, starting from zero state, g_2^0 term has reached -1600γ during
the last one and a half centuries. During the last several centuries,
on the other hand, the largest root-mean-square residuals of the present
time invariant model, which is considered to give an estimate of any
possible time variation of the standing and the drifting field, only
amounts to 500γ. It indicates that the two types of field separated
here are very stable and steady. Therefore the steadily drifting field
may be associated with such a large scale fluid motion that may have
interaction with the strong toroidal field in the deep part of the core
rather than a turbulent motion near the surface of the core.

Another noteworthy property of the secular variation derived from
the present study is non-existence of interference between the standing
and the drifting field. As was seen in the previous section, somewhat
complicated features of the secular variation in the non-dipole field can
be well accounted for by a simple linear superposition of the two types
of field and we need not consider any complicated non-linear interaction
between the two. This seems to rule out the possibility that the stand-
ing field may have something to do with the mechanism of producing
the drifting field, and to suggest that they are of separate origin.

The non-dipole fields that may be expressed by spherical harmonic
terms lower than $n=m=6$ have so far been believed to originate from
within the core, mainly because they are subjected to such rapid vari-
ations as may be difficult to ascribe their sources to the solid part of
the earth. However, the standing field separated in this paper does
not seem to have undergone any perceptible variation during the last
several centuries. As far as small regional anomalies are concerned,
such as the negative near the Aleutian Islands in the North Pacific and
the positive anomaly in the Central Pacific, they would have changed
their intensity during the period treated here, if they originated from
the liquid core, because, even if hydrodynamic conditions are ignored,
free decay time of the magnetic field for these small anomalies would
be of the order of several hundred years. Since the regional anomalies

having short wave lengths mostly originate in the crust,[8] the above small anomalies are suspected of having their sources within the solid part of the earth, in the crust or in the upper mantle, though it is not certain as yet whether the whole part of the standing field should be ascribed to the crustal origin or not.

We express our thanks to Prof. T. Rikitake for his helpful discussion.

---

5. 地球磁場の移動性部分と停滞性部分の分離

地震研究所 { 行 武 　 毅
立 中 ひろ子

17世紀にさかのぼって，地球磁場の球函数展開係数をもちい，地球磁場を移動性部分と停滞性部分とに分離した．移動性磁場は球函数の低次の項で構成され，比較的単純な分布をしている．停滞性磁場の分布は，これに比べると複雑である．

ここで分離された2種類の磁場を重ね合せることによって，過去数世紀にわたる地球磁場の変化を，充分よく近似できることが確められた．蒙古地方の磁気異常の年間50γにおよぶ急速な成長も，2種類の磁場の単純な重ね合せで説明できることがわかった．移動性磁場と停滞性磁場との間に，相互作用が認められないのは注目すべきことで，両者の発生機構が全く異るのではないかと考えられる．

---

8) L. R. ALLDREDGE, G. D. V. VOORHIS and T. M. DAVIS, "A Magnetic Profile around the World," *J. Geophys. Res.*, **68** (1963), 3679-3692.